"Simulating tubulin-associated unit transport in an axon: using bootstrapping for estimating confidence intervals of best fit parameter values obtained from indirect experimental data"

Proceedings of the Royal Society A

I. A. Kuznetsov[(a), (b)] and A. V. Kuznetsov[(c)]

[(a)]Perelman School of Medicine, University of Pennsylvania, Philadelphia, PA 19104, USA

[(b)]Department of Bioengineering, University of Pennsylvania, Philadelphia, PA 19104, USA

[(c)]Dept. of Mechanical and Aerospace Engineering, North Carolina State University, Raleigh, NC 27695-7910, USA; e-mail: avkuznet@ncsu.edu

Supplementary material

Full model, dimensionless equations for the steady-state formulation

Black et al. [40] reports results of a fluorescent study and therefore Fig. 7D shows the relative amount of tau in the axon; Eqs. (2.1)-(2.7), however, contain absolute concentrations of tau. To overcome this difficulty, we recast governing equations into the dimensionless form (this also allowed us to minimize the number of parameters in the equations). We introduced dimensionless tau concentrations by dividing all tau concentrations by the total tau concentration at the axon hillock, for example:

$$n_a = \frac{n_a^*}{n_{tot,x=0}^*}. \tag{S1}$$

The dimensionless forms of Eqs. (2.1)-(2.7) are

$$-\frac{dn_a}{dx} - \gamma_{10} n_a + \gamma_{01} n_{a0} = 0, \tag{S2}$$

$$v_r \frac{dn_r}{dx} - \gamma_{10} n_r + \gamma_{01} n_{r0} = 0, \tag{S3}$$

$$-\left(\gamma_{01} + \gamma_{ar} + \gamma_{off,a}\right) n_{a0} + \gamma_{10} n_a + \gamma_{ra} n_{r0} + \gamma_{on,a} n_{free} = 0, \tag{S4}$$

$$-\left(\gamma_{01} + \gamma_{ra} + \gamma_{off,r}\right) n_{r0} + \gamma_{10} n_r + \gamma_{ar} n_{a0} + \gamma_{on,r} n_{free} = 0, \tag{S5}$$

$$D_{free} \frac{d^2 n_{free}}{dx^2} + \gamma_{off,a} n_{a0} + \gamma_{off,r} n_{r0} - \left(\gamma_{on,a} + \gamma_{on,r} + \gamma_{free \to st} + \gamma_{free \to dif}\right) n_{free} + \gamma_{st \to free} n_{st} + \gamma_{dif \to free} n_{dif}$$

$$-n_{free}\ln(2)=0\,, \tag{S6}$$

$$-\left(\gamma_{st\to free}+\gamma_{st\to dif}\right)n_{st}+\gamma_{free\to st}n_{free}+\gamma_{dif\to st}n_{dif}=0\,, \tag{S7}$$

$$D_{mt}\frac{d^2n_{dif}}{dx^2}-\left(\gamma_{dif\to free}+\gamma_{dif\to st}\right)n_{dif}+\gamma_{free\to dif}n_{free}+\gamma_{st\to dif}n_{st}=0\,. \tag{S8}$$

In Eqs. (S2)-(S8), the dimensionless linear coordinate was defined as:

$$x=\frac{x^*}{v_a^*T_{1/2}^*}\,. \tag{S9}$$

The dimensionless kinetic constants were defined by multiplying a corresponding kinetic constant by $T_{1/2}^*$, for example:

$$\gamma_{10}=\gamma_{10}^*T_{1/2}^* \tag{S10}$$

and other dimensionless parameters were defined as follows:

$$D_{free}=\frac{D_{free}^*}{v_a^{*2}T_{1/2}^*},\ D_{mt}=\frac{D_{mt}^*}{v_a^{*2}T_{1/2}^*},\ v_r=\frac{v_r^*}{v_a^*}\,. \tag{S11}$$

The values of dimensionless parameters can be easily obtained from Eqs. (S10), (S11) and Table 2.

Eqs. (2.10)-(2.12) can now be re-written in the dimensionless form as:

$$j_{tot}=j_{dif}+j_{mm}\,, \tag{S12}$$

where

$$j_{dif}=-D_{free}\frac{dn_{free}}{dx}-D_{mt}\frac{dn_{dif}}{dx} \tag{S13}$$

and

$$j_{mm}=n_a-v_rn_r\,. \tag{S14}$$

In Eqs. (S12)-(S14)

$$j_{tot}=\frac{j_{tot}^*}{n_{tot,x=0}^*v_a^*},\ \ j_{dif}=\frac{j_{dif}^*}{n_{tot,x=0}^*v_a^*},\ \ j_{mm}=\frac{j_{mm}^*}{n_{tot,x=0}^*v_a^*}\,. \tag{S15}$$

The dimensionless form of Eq. (2.13) then is

$$v_{av} = \frac{j_{tot}}{n_{tot}}, \tag{S16}$$

where

$$v_{av} = \frac{v_{av}^*}{v_a^*}. \tag{S17}$$

Dimensionless boundary conditions

The dimensionless boundary conditions at the axon hillock are

$$\text{At } x = 0: \qquad n_{free} = n_{free,x=0}, \quad j_{tot} = j_{tot,x=0}, \qquad n_{dif} = n_{dif,x=0}, \tag{S18a,b,c}$$

where

$$n_{free,x=0} = \frac{n_{free,x=0}^*}{n_{tot,x=0}^*}, \qquad n_{dif,x=0} = \frac{n_{dif,x=0}^*}{n_{tot,x=0}^*}, \qquad j_{tot,x=0} = \frac{j_{tot,x=0}^*}{n_{tot,x=0}^* v_a^*}. \tag{S19}$$

The dimensionless boundary conditions at the axon terminal are

$$\text{At } x = L: \qquad \frac{dn_{free}}{dx} = 0, \qquad j_{tot} = j_{tot,x=L}, \qquad \frac{dn_{dif}}{dx} = 0, \tag{S20a,b,c}$$

where

$$L = \frac{L^*}{v_a^* T_{1/2}^*}, \qquad j_{tot,x=L} = \frac{j_{tot,x=L}^*}{n_{tot,x=0}^* v_a^*}. \tag{S21}$$

The detailed form of Eq. (S20b) is

$$-D_{free}\frac{dn_{free}}{dx} - D_{mt}\frac{dn_{dif}}{dx} + n_a - v_r n_r = A\left(1 - \exp\left[-\frac{\log(2)}{\gamma_{ar}}\right]\right)n_a. \tag{S22}$$

Simplified model, dimensionless equations for the steady-state formulation

The dimensionless forms of Eqs. (2.19)-(2.25) are

$$-\frac{dn_a}{dx} - \gamma_{10} n_a + \gamma_{01} n_{a0} = 0, \tag{S23}$$

$$v_r \frac{dn_r}{dx} - \gamma_{10} n_r + \gamma_{01} n_{r0} = 0\,, \tag{S24}$$

$$-\gamma_{01} n_{a0} + \gamma_{10} n_a + \gamma_{ra} n_{r0} + \gamma_{on,a} n_{free} = 0\,, \tag{S25}$$

$$-\left(\gamma_{01} + \gamma_{ra}\right) n_{r0} + \gamma_{10} n_r = 0\,, \tag{S26}$$

$$D_{free} \frac{d^2 n_{free}}{dx^2} - \gamma_{on,a} n_{free} + \gamma_{dif \to free} n_{dif} - n_{free} \ln(2) = 0\,, \tag{S27}$$

$$n_{st} = 0\,, \tag{S28}$$

$$D_{mt} \frac{d^2 n_{dif}}{dx^2} - \gamma_{dif \to free} n_{dif} = 0\,. \tag{S29}$$

Boundary conditions given by Eqs. (S18), (S20) stand; since $\gamma_{ar} \to 0$ in the simplified model, Eq. (S22) can be simplified as:

$$-D_{free} \frac{dn_{free}}{dx} - D_{mt} \frac{dn_{dif}}{dx} + n_a - v_r n_r = A n_a\,. \tag{S30}$$

Dimensionless equation for the objective function

The dimensionless form of Eq. (2.18) is

$$err = \sum_{i=1}^{N} \left(n_{tot,i} - n_{tot,exper,i}\right)^2 + \omega_1 v_a^{*2} \sum_{i=1}^{N} \left(v_{av,i} - \frac{0.00345\,\mu\text{m/s}}{v_a^*} \right)^2 + \omega_2 \left(\%\text{bound}\big|_{x=L/2} - 100\right)^2\,. \tag{S31}$$

Solutions for n_{free}^* and n_{dif}^* of the simplified model

The solution of Eq. (2.23) subject to boundary conditions (2.14a) and (2.15a) is

$$n^*_{free} = \{2 D^*_{mt} n^*_{dif,x=0} T^*_{1/2} \gamma^*_{dif\to free} (-\cosh\left[x\sqrt{\frac{T^*_{1/2}\gamma^*_{on,a} + \ln(2)}{D^*_{free} T^*_{1/2}}} \right]$$
$$+\cosh\left[(L-x)\sqrt{\frac{\gamma^*_{dif\to free}}{D^*_{mt}}} \right] \mathrm{sech}\left[L\sqrt{\frac{\gamma^*_{dif\to free}}{D^*_{mt}}} \right] \qquad \text{(S32)}$$
$$+\sinh\left[x\sqrt{\frac{T^*_{1/2}\gamma^*_{on,a} + \ln(2)}{D^*_{free} T^*_{1/2}}} \right] \tanh\left[L\sqrt{\frac{T^*_{1/2}\gamma^*_{on,a} + \ln(2)}{D^*_{free} T^*_{1/2}}} \right])\}$$
$$/\left\{ D^*_{mt}(2T^*_{1/2}\gamma^*_{on,a} + \ln(4)) - 2D^*_{free} T^*_{1/2} \gamma^*_{dif\to free} \right\}.$$

The solution of Eq. (2.25) subject to boundary conditions (2.14c) and (2.15c) is

$$n^*_{dif} = n^*_{dif,x=0} \cosh\left[(L-x)\sqrt{\frac{\gamma^*_{dif\to free}}{D^*_{mt}}} \right] \mathrm{sech}\left[L\sqrt{\frac{\gamma^*_{dif\to free}}{D^*_{mt}}} \right]. \qquad \text{(S33)}$$

Effect of the weighting factor ω_1 on solutions of the simplified model

Fig. S1 shows the effects of the weighting factor ω_1 in Eq. (2.18) on the total tau concentration and the tau average velocity.

Comparison between solutions of the full and simplified models for seven components of the total tau concentration and the percentage of MT-bound tau

In order to justify the reduction from to the full to the simplified model we plotted all seven components of the total tau concentration (Figs. S2, S3, S4, and S5a). The concentrations of tau in the motor-driven states slowly increase toward the axon terminal (Fig. S2), which suggests that motor-driven transport of tau is relevant over the whole axon length. The concentrations of tau in the pausing states are much larger (Fig. S3), which is because in slow axonal transport cargo is pausing most of the time (according to [27], tau spends 73% of the time in the pausing states). Tau concentrations in the pausing states also increase toward the terminal because running and pausing tau must be in equilibrium. The concentration of cytosolic tau is quite low (Fig. S4a); the same applies to the concentration of stationary MT-bound tau (Fig. S4b). The concentration of MT-bound tau diffusing along MTs drops quickly and is significant only near the soma (Fig. S5a). These findings suggest that diffusion is only significant close to the soma. In terms of the agreement between the full and simplified model solutions, the components of tau concentration predicted by the two models are almost identical. The only exception is the distribution of the

stationary MT-bound tau (Fig. S4b). According to the simplified model n_{st} is equal to zero (Eq. (2.24)), while the full model predicts a quickly decreasing distribution of n_{st} (solid line in Fig. 4b). Since the percentage of stationary MT-bound tau in the total tau concentration is small, this discrepancy does not have any significant impact on the agreement between the total tau concentration predicted by the full and simplified models (Fig. 3a). Almost all tau is MT-bound (Fig. S5b), except in a small region in the beginning of the axon where some cytoplasmic tau is present (Fig. S4a).

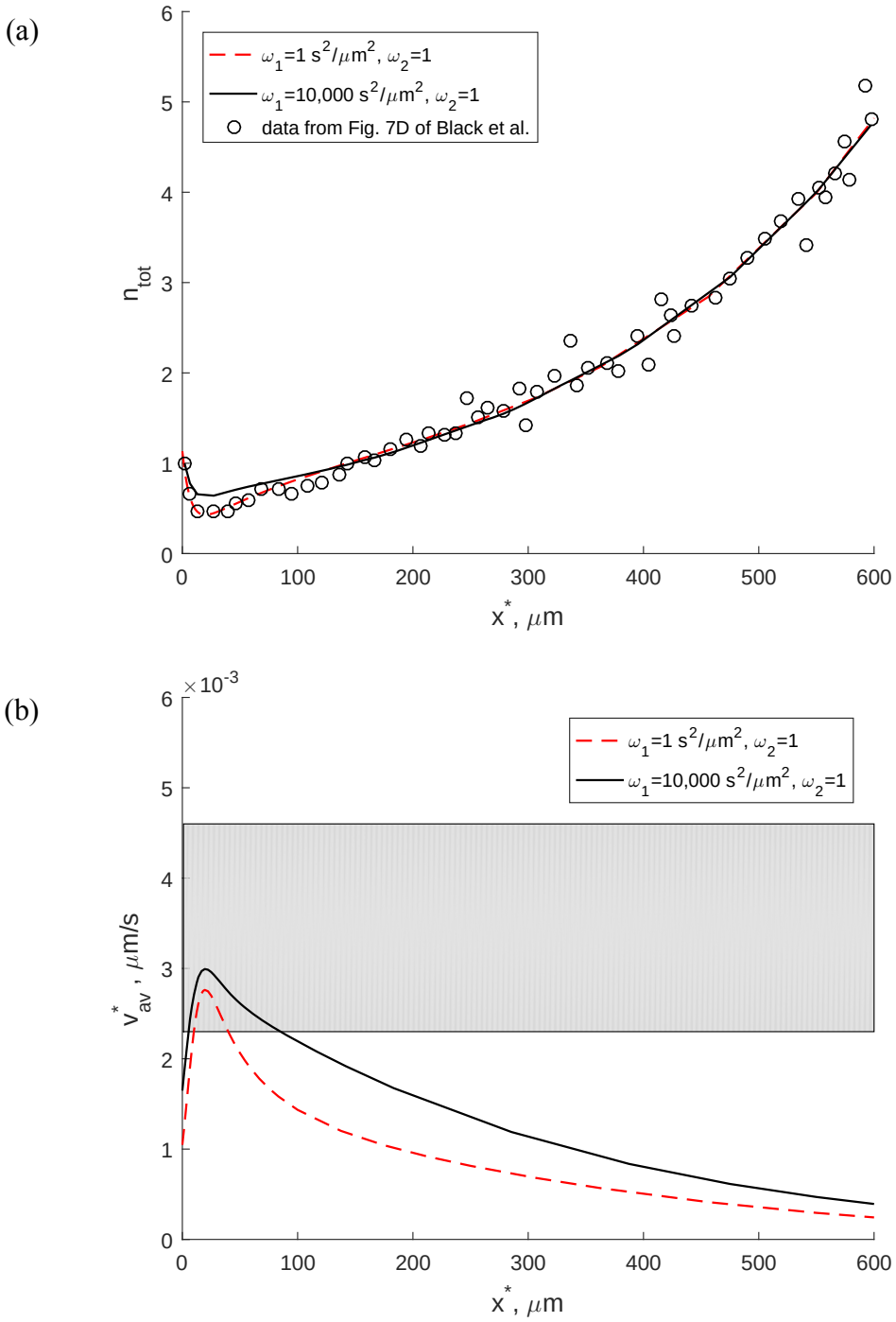

Fig. S1. The effect of the weighting factor ω_1 in the objective function defined by Eq. (2.18) on predicted distributions of (a) the total tau concentration and (b) the tau average velocity.

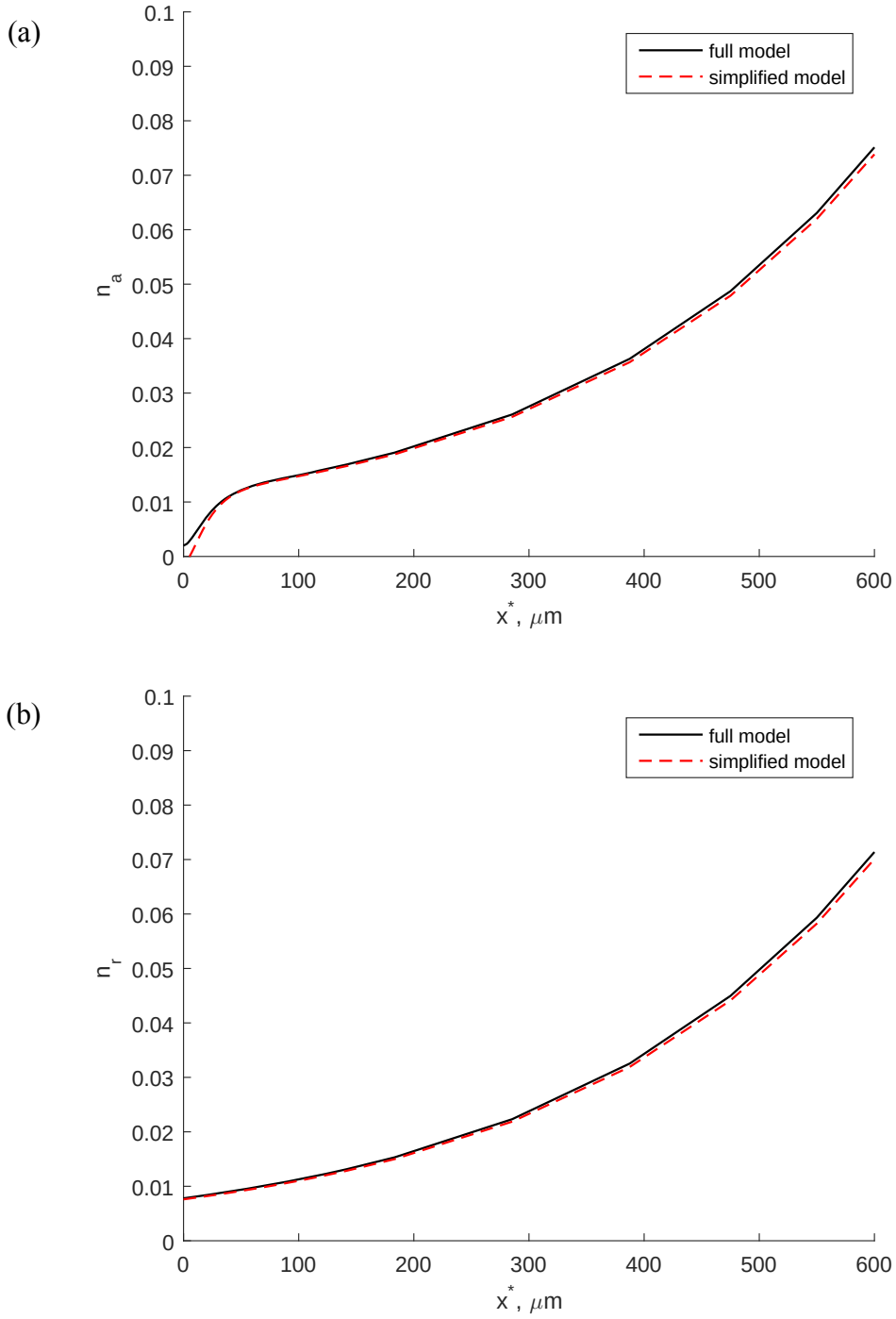

Fig. S2. (a) Dimensionless concentration of on-track motor-driven tau moving along MTs anterogradely vs position in the axon. (b) Dimensionless concentration of on-track motor-driven tau moving along MTs retrogradely vs position in the axon. ($\omega_1 = 10,000$ s^2/μm^2, $\omega_2 = 1$).

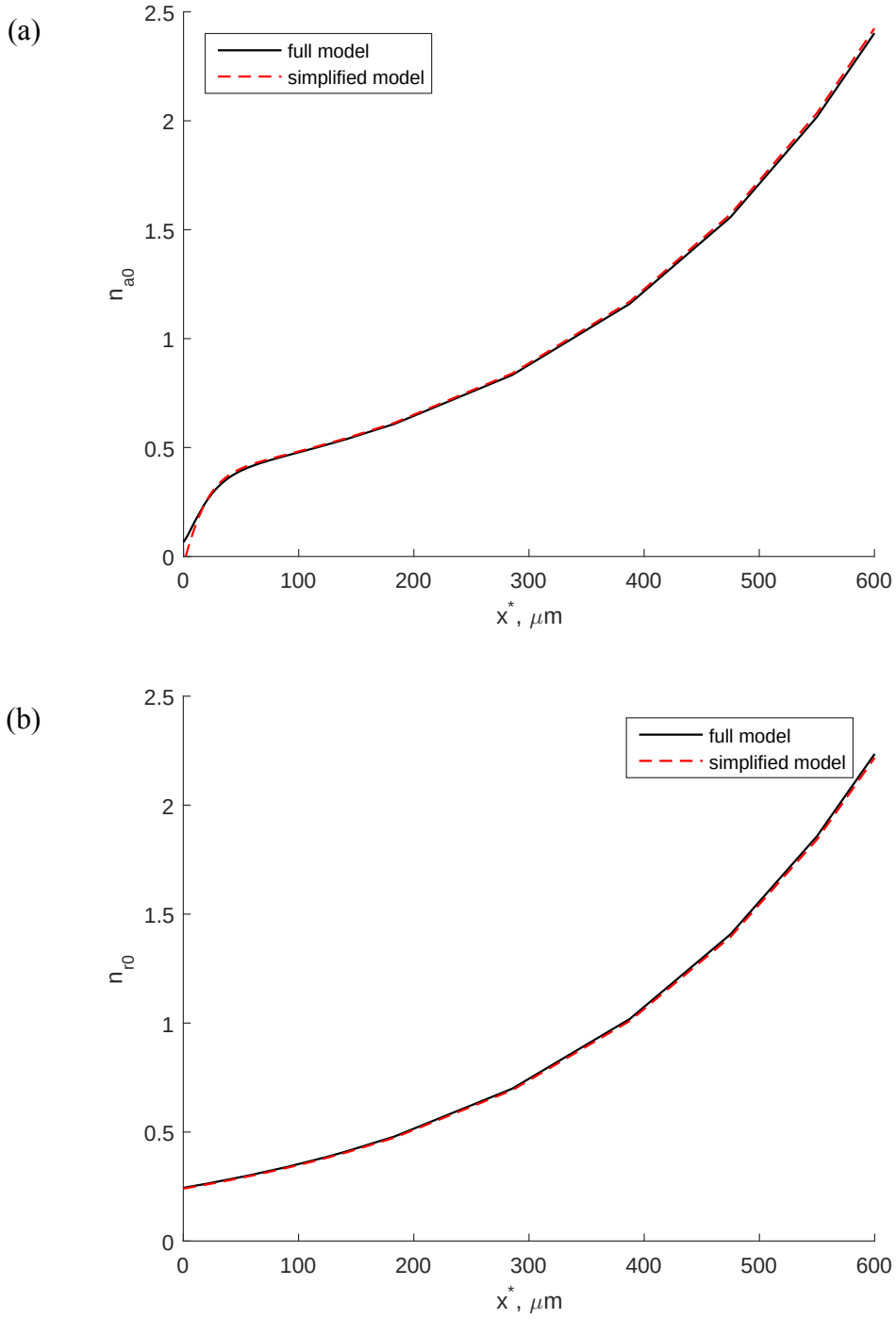

Fig. S3. (a) Dimensionless concentration of pausing on-track tau associated with anterograde motors vs position in the axon. (b) Dimensionless concentration of pausing on-track tau associated with retrograde motors vs position in the axon. ($\omega_1 = 10,000$ s^2/μm^2, $\omega_2 = 1$).

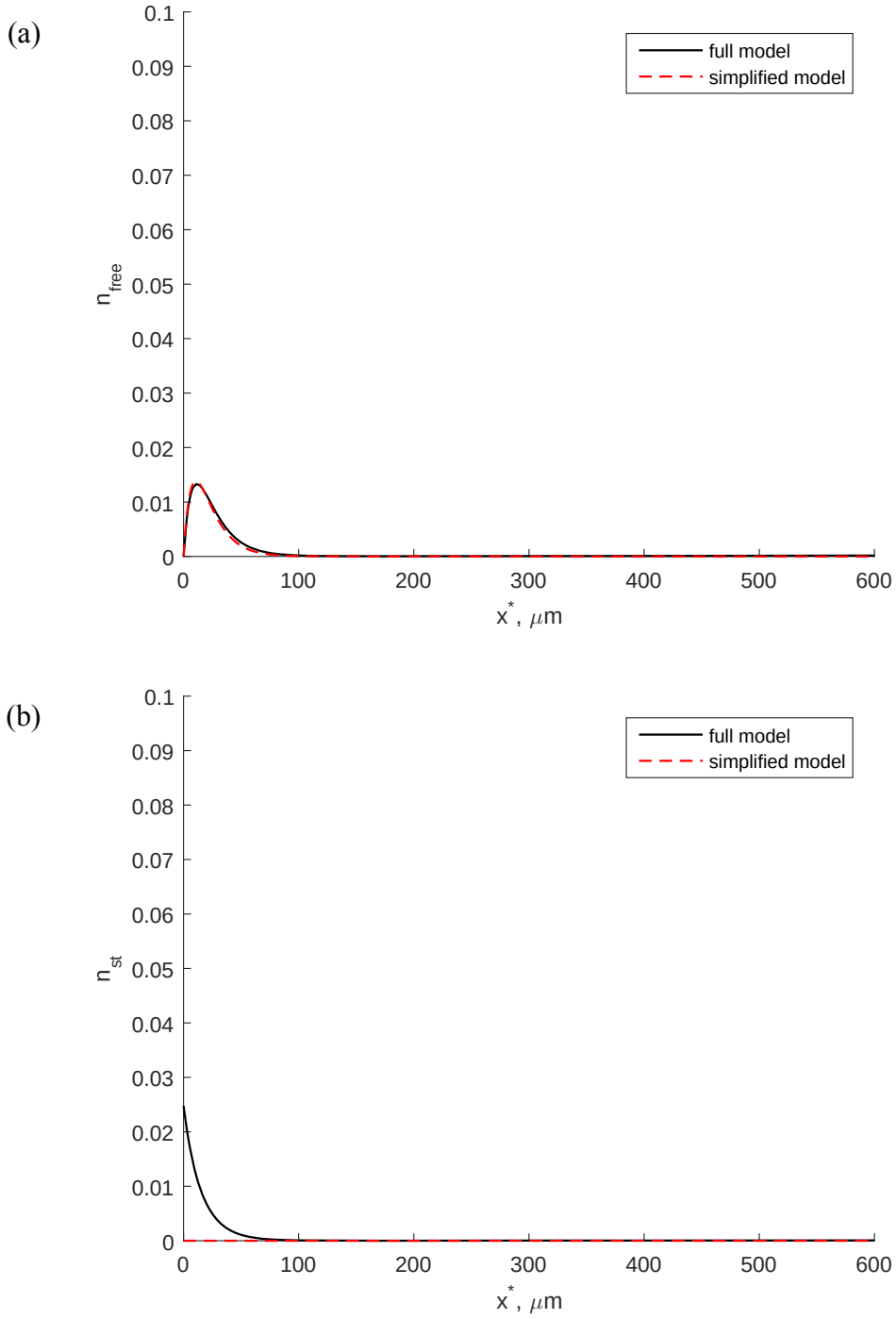

Fig. S4. (a) Dimensionless concentration of free (diffusing) tau vs position in the axon. (b) Dimensionless concentration of stationary tau bound to MTs, no association with motors, vs position in the axon. ($\omega_1 = 10{,}000$ s^2/μm^2, $\omega_2 = 1$).

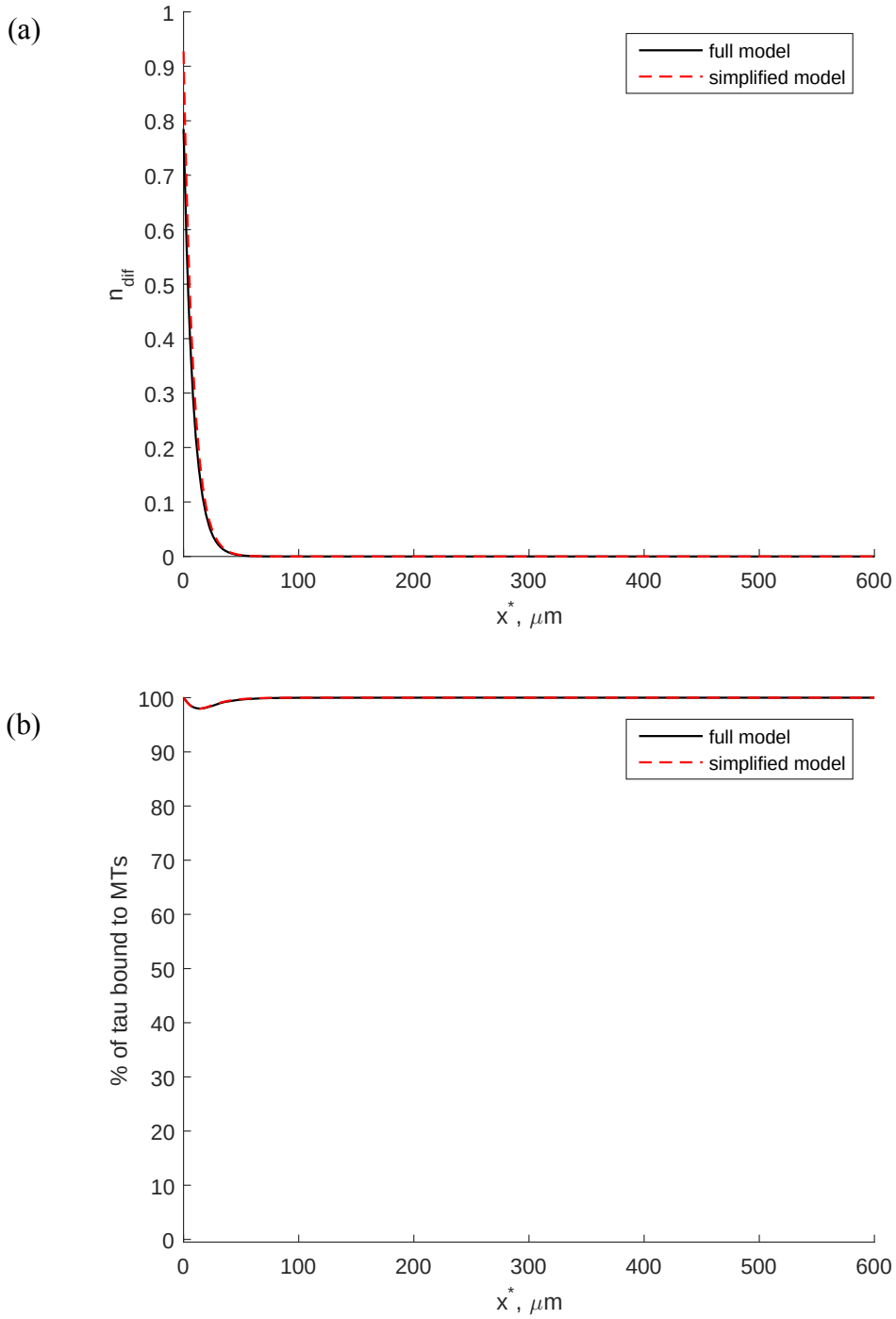

Fig. S5. (a) Dimensionless concentration of tau diffusing along MTs, no association with motors. (b) Percentage of MT-bound tau vs position in the axon. ($\omega_1 = 10,000$ $s^2/\mu m^2$, $\omega_2 = 1$).

Solutions for a surrogate data set

Figs. S6-S11 show how the solutions for a surrogate data set differ from the solutions for the actual data set. We show solutions for one surrogate data set for which the minimized value of the objective function, defined by Eq. (2.18), is 4.333 (see the histogram of the minimized value of the objective function in Fig. 6). The minimized value of the objective function for the actual experimental data is 3.272. The total tau concentration for the surrogate data set is shown by crosses in Fig. S10a. It is interesting that for the surrogate data set diffusion contributes to tau transport for up to 200 μm from the soma rather than up to 100 μm from the soma for the actual data set (Figs. S11a, S11b).

(a)

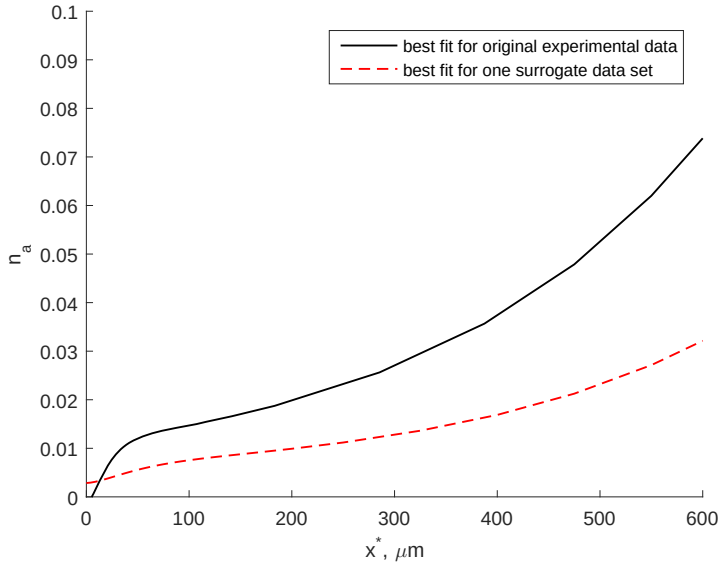

(b)

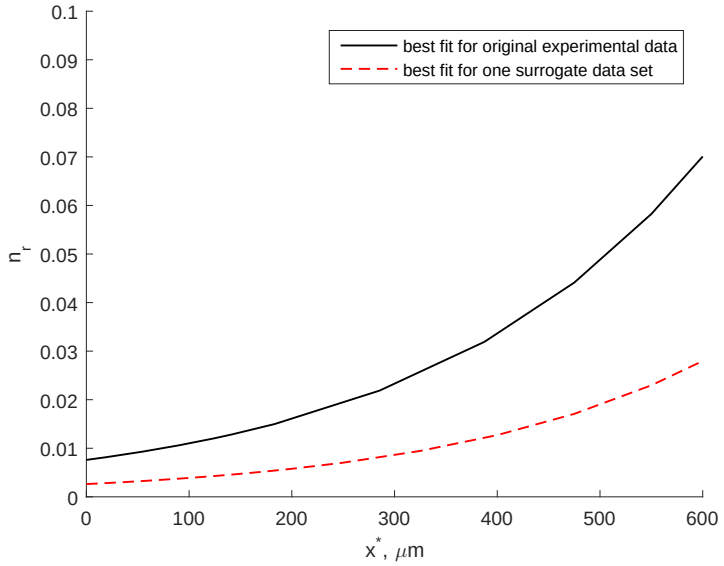

Fig. S6. Similar to Fig. S2, but now showing predictions of the simplified model for one surrogate data set obtained by resampling residuals (out of 5,000 surrogate data sets used to produce the histograms). Predictions of the simplified model for the actual experimental data are also shown for comparison. The minimized value of the objective function, defined by Eq. (2.18), for the actual experimental data is 3.272 while the minimized value of the objective function for the surrogate data set is 4.333. (a) Dimensionless concentration of on-track motor-driven tau moving along MTs anterogradely vs position in the axon. (b) Dimensionless concentration of on-track motor-driven tau moving along MTs retrogradely vs position in the axon. ($\omega_1 = 10,000$ $s^2/\mu m^2$, $\omega_2 = 1$).

(a)

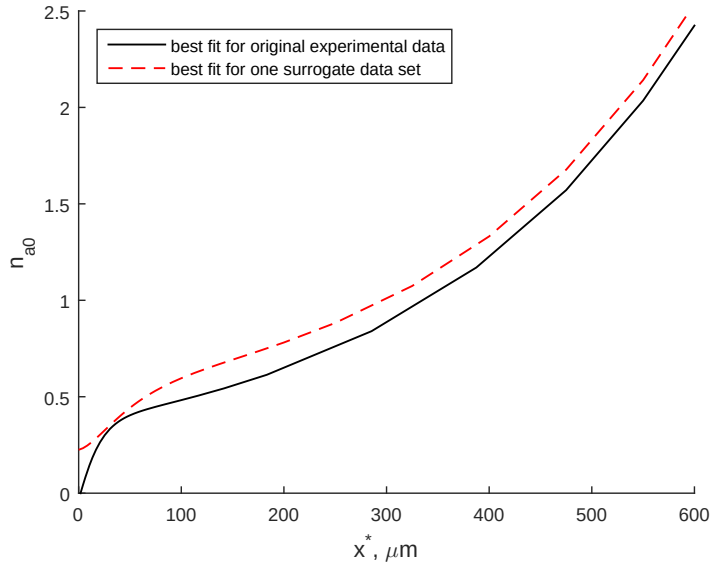

(b)

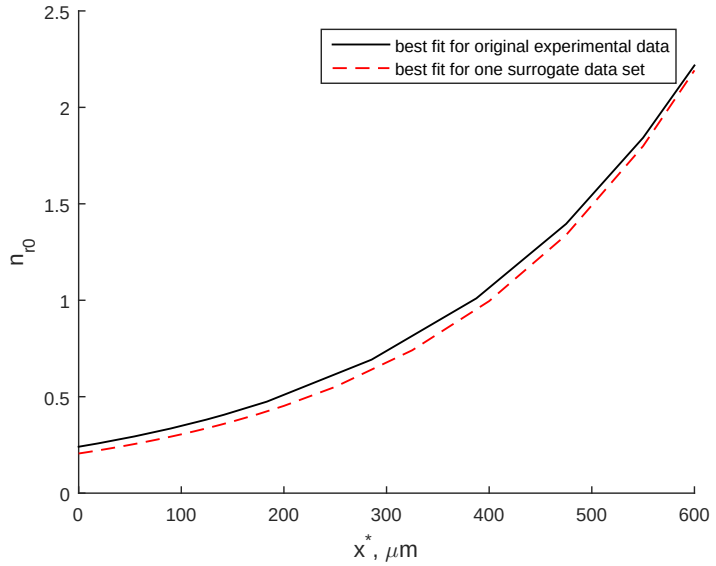

Fig. S7. Similar to Fig. S3, but now showing predictions of the simplified model for one surrogate data set obtained by resampling residuals (out of 5,000 surrogate data sets used to produce the histograms). Predictions of the simplified model for the actual experimental data are also shown for comparison. (a) Dimensionless concentration of pausing on-track tau associated with anterograde motors vs position in the axon. (b) Dimensionless concentration of pausing on-track tau associated with retrograde motors vs position in the axon. ($\omega_1 = 10,000$ s^2/μm^2, $\omega_2 = 1$).

(a)

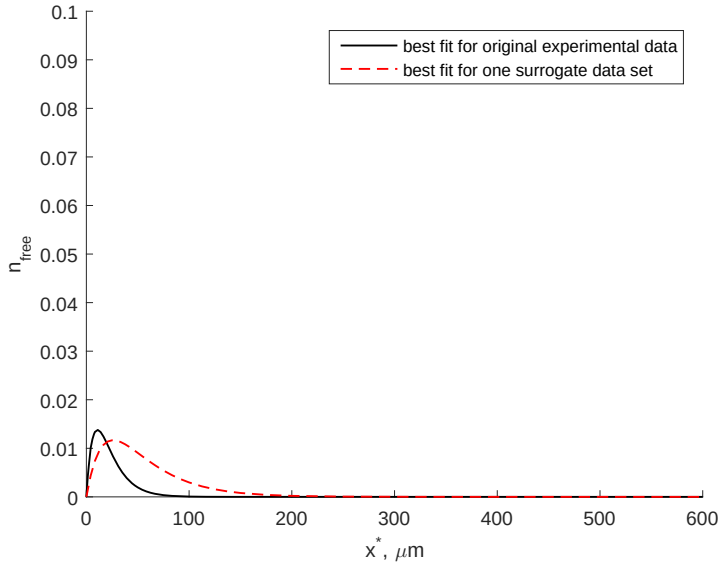

(b)

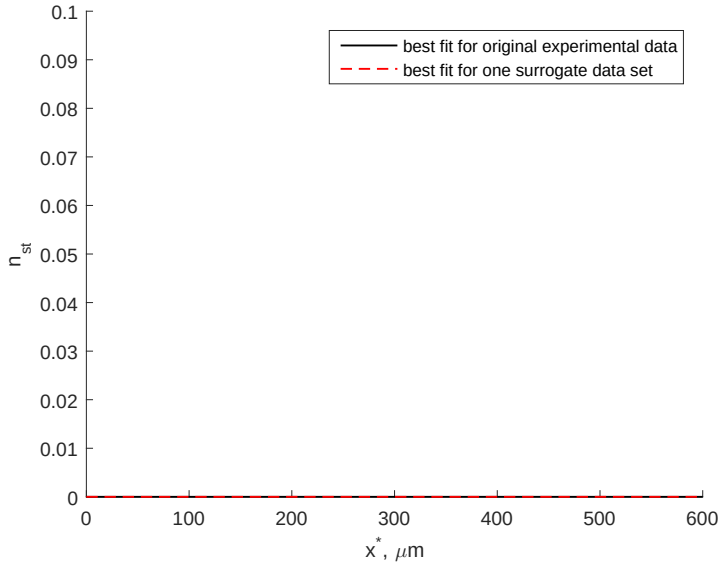

Fig. S8. Similar to Fig. S4, but now showing predictions of the simplified model for one surrogate data set obtained by resampling residuals (out of 5,000 surrogate data sets used to produce the histograms). Predictions of the simplified model for the actual experimental data are also shown for comparison. (a) Dimensionless concentration of free (diffusing) tau vs position in the axon. (b) Dimensionless concentration of stationary tau bound to MTs, no association with motors, vs position in the axon. ($\omega_1 = 10,000$ s^2/μm^2, $\omega_2 = 1$).

(a)

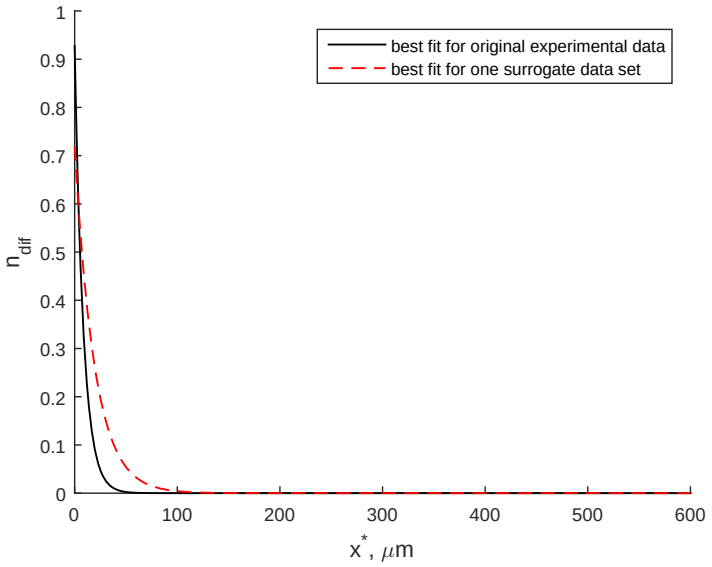

(b)

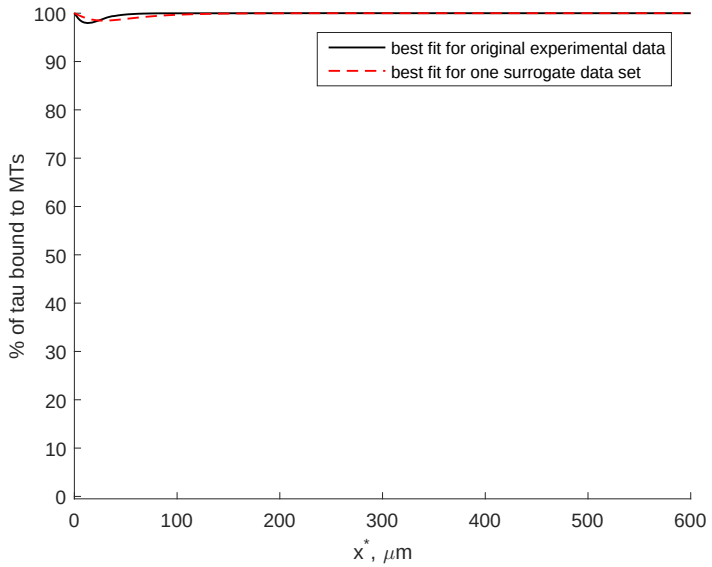

Fig. S9. Similar to Fig. S5, but now showing predictions of the simplified model for one surrogate data set obtained by resampling residuals (out of 5,000 surrogate data sets used to produce the histograms). Predictions of the simplified model for the actual experimental data are also shown for comparison. (a) Dimensionless concentration of tau diffusing along MTs, no association with motors. (b) Percentage of MT-bound tau vs position in the axon. ($\omega_1 = 10{,}000$ $s^2/\mu m^2$, $\omega_2 = 1$).

(a)

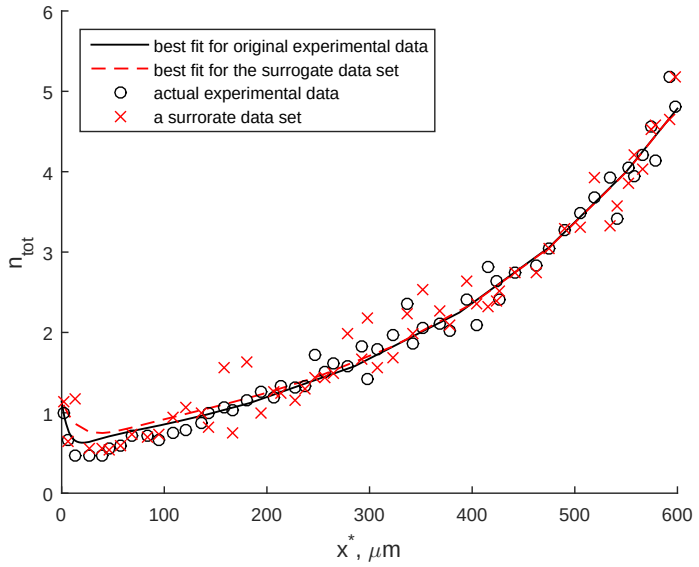

(b)

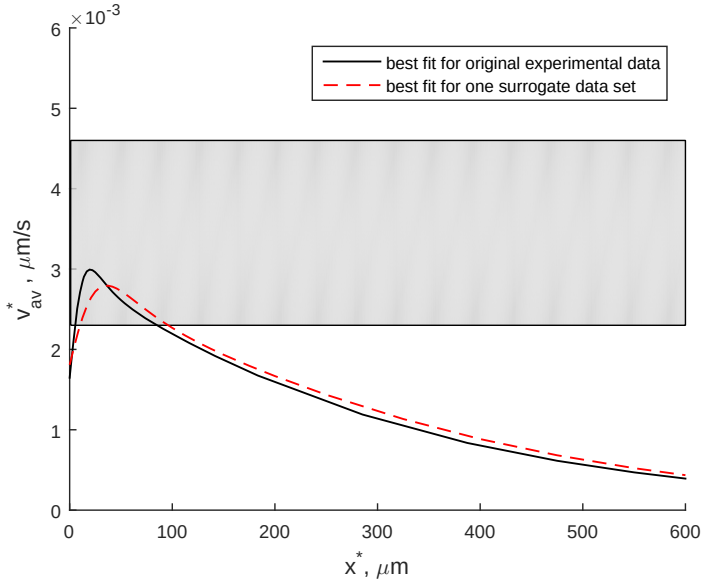

Fig. S10. Similar to Fig. 3, but now showing predictions of the simplified model for one surrogate data set obtained by resampling residuals (out of 5,000 surrogate data sets used to produce the histograms). Predictions of the simplified model for the actual experimental data are also shown for comparison. (a) Dimensionless total concentration of tau vs position in the axon. The actual experimental data for the total tau concentration are shown by open circles and the surrogate data are shown by crosses. (b) Tau average velocity vs position in the axon. A horizontal band shows the range of the average velocity of tau protein reported in [51]. ($\omega_1 = 10,000$ s^2/μm^2, $\omega_2 = 1$).

(a)

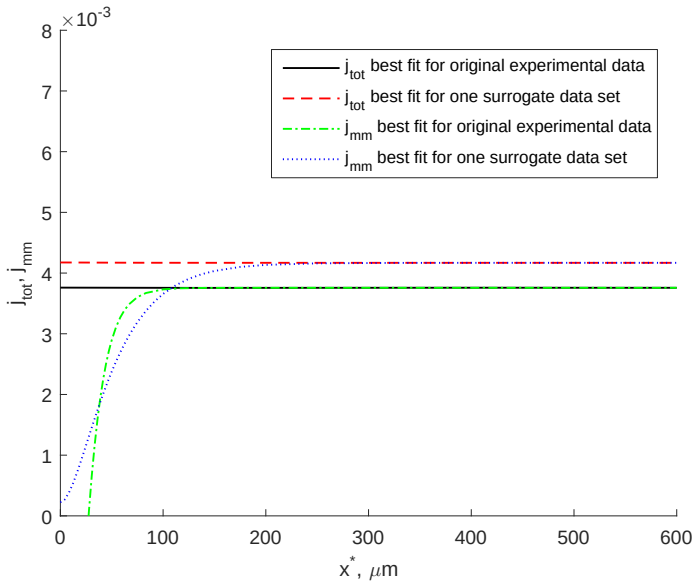

(b)

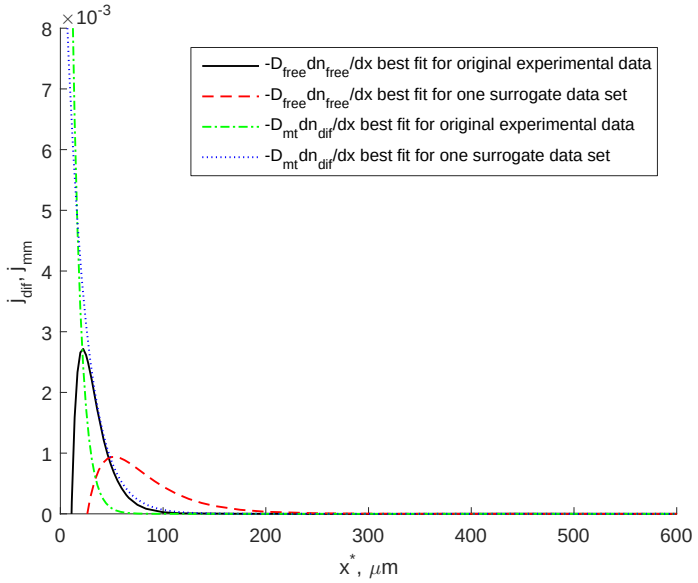

Fig. S11. Similar to Fig. 4, but now showing predictions of the simplified model for one surrogate data set obtained by resampling residuals (out of 5,000 surrogate data sets used to produce the histograms). Predictions of the simplified model for the actual experimental data are also shown for comparison. (a) Total dimensionless tau flux and molecular motor-driven tau flux vs position in the axon. (b) Two components of the dimensionless diffusion-driven tau flux, due to diffusion of cytoplasmic tau, $-D_{free}\dfrac{dn_{free}}{dx}$, and due to diffusion of MT-bound tau, $-D_{mt}\dfrac{dn_{dif}}{dx}$, vs position in the axon. ($\omega_1 = 10{,}000$ s^2/μm^2, $\omega_2 = 1$).